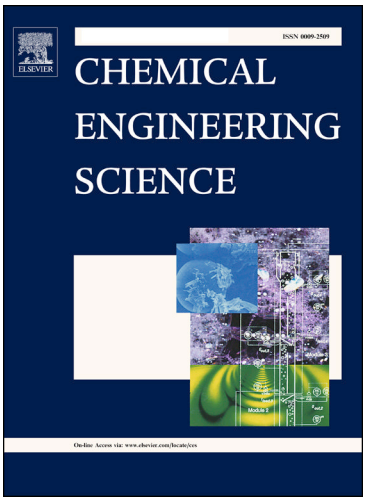

Dynamic changes in gas-liquid mass transfer during Taylor flow in long serpentine square microchannels

Peng Zhang, Chaoqun Yao, Haiyun Ma, Nan Jin, Xunli Zhang, Hongying Lü, Yuchao Zhao

PII: S0009-2509(18)30080-0
DOI: https://doi.org/10.1016/j.ces.2018.02.018
Reference: CES 14042

To appear in: *Chemical Engineering Science*

Received Date: 5 November 2017
Revised Date: 11 February 2018
Accepted Date: 13 February 2018

Please cite this article as: P. Zhang, C. Yao, H. Ma, N. Jin, X. Zhang, H. Lü, Y. Zhao, Dynamic changes in gas-liquid mass transfer during Taylor flow in long serpentine square microchannels, *Chemical Engineering Science* (2018), doi: https://doi.org/10.1016/j.ces.2018.02.018

Dynamic changes in gas-liquid mass transfer during Taylor flow in long serpentine square microchannels

Peng Zhang[a,ξ], Chaoqun Yao[b,ξ], Haiyun Ma[a], Nan Jin[a], Xunli Zhang[c], Hongying Lü[a], Yuchao Zhao[a,*]

[a] Shandong Collaborative Innovation Center of Light hydrocarbon transformation and utilization, College of Chemistry & Chemical Engineering, Yantai University, Yantai 264005, China

[b] Dalian National Laboratory for Clean Energy, Dalian Institute of Chemical Physics, Chinese Academy of Sciences, Dalian116023, China

c Faculty of Engineering and the Environment & Institute for Life Sciences, University of Southampton, Southampton SO17 1BJ, UK

[ξ] The authors contribute equally to the paper

Abstract

The present work focuses on the hydrodynamics variation and mass transfer characteristics of Taylor flow along long serpentine microchannels with a square cross-section. The volumetric mass transfer coefficient (k_La) is regarded as the transient change value to characterize the gas-liquid mass transfer process of CO_2 in water. All experimental data of Taylor bubble are obtained from 1,000 continuously captured images. An online high-speed imaging method and the unit cell model are adopted in this study. The effects of gas and liquid flow rates, together with microchannel geometry are investigated on Taylor bubble characteristics in terms of length, velocity and the mass transfer performance.

Taylor bubble length shrinks and subsequently plateaus out along the flow direction from the T-junction, resulting in the decrease in Taylor bubble velocity. k_La in a unit cell gradually decreases along the serpentine microchannel, and increases as the channel cross-sectional area decreases. As the gas flow rate increases under a given liquid flow rate, a critical point is found for the evolution of k_La and k_L (that is the

* Corresponding Author. Tel: +86 535 6901717.
E-mail address: yczhao@ytu.edu.cn (Y. Zhao).

liquid phase mass transfer coefficient). The results indicate that the contribution of the circulation in the liquid slug to k_L is dominant before the critical point compared to the leakage flow in the liquid film. All these findings in this work give important information to understand the dynamic change in gas-liquid Taylor flow mass transfer within microchannels. They will serve as basis for designing and optimizing gas-liquid multiphase microreactors in the future.

Keywords:

Microchannel; Gas-liquid; Mass transfer; Carbon dioxide; Taylor flow

1. Introduction

Microchannel reactors or microfluidic devices are gaining considerable attention from academia and industry for carrying out gas-liquid multiphase processes due to their capability to intensify transport processes, improve process control, increase safety and enhance compactness (Hessel et al., 2005; Günther et al., 2006; Yang et al., 2014; Gemoets et al., 2016; Li et al., 2017). However, whether microchannel reactors are viable alternatives to the commonly-used macroscale multiphase reactors largely depends on the exploitation of their characteristics of hydrodynamics and mass transfer to be beneficial to the reaction process, the design and the operational optimization of the reactor (Salman et al., 2007; Zhao et al., 2013; Abolhasani et al., 2015; Sobieszuk and Napieralska, 2016).

Gas-liquid multiphase flow through microchannels is considerably different from conventional macroscale channels, as the flow pattern of microscale two-phase flow predominated by Taylor flow or slug flow (van Steijn et al., 2007; Yue et al., 2008; Shao et al., 2009; Kashid et al., 2011). Taylor flow is typically characterized by the presence of elongated gas bubbles with a length longer than the channel diameter or width, where such bubbles flow along the microchannel and are separated from each other by liquid slugs. These bubbles are also separated from the channel wall with a thin liquid film. Fig. 1 illustrates schematically a typical gas-liquid two-phase Taylor flow in a microchannel.

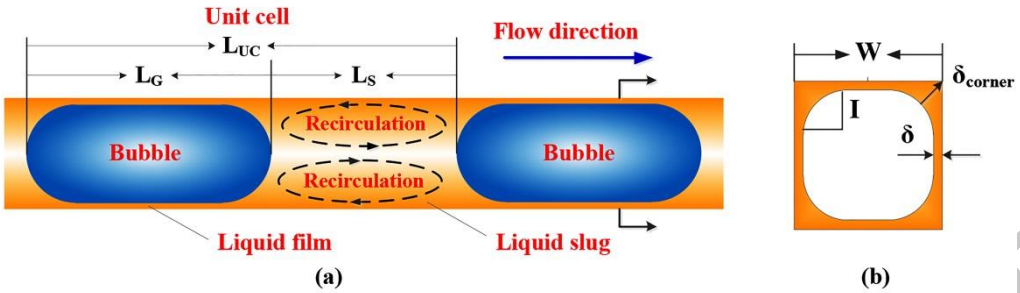

Fig. 1. Schematic of typical gas-liquid two-phase Taylor flow in a microchannel (a) Taylor bubble and slug in a unit cell; (b) Cross-section of Taylor bubble

It has been well observed that in Taylor flow, there is a recirculation within the liquid slug mainly due to the difference in the velocity field between the gas bubble and the liquid slug. It is the recirculation that can significantly enhance local mixing leading to augmented heat and mass transfer (i) in the radial direction within the liquid slug, and (ii) in the axial dispersion across the gas-liquid interface (Kececi et al. 2009; Su et al. 2012). In addition, the axial dispersion can be greatly reduced due to the segmentation of gas bubbles and liquid slugs compared to laminar flow (Pedersen and Horvath, 1981; Jia and Zhang, 2016). Moreover, the mass transfer or mixing between liquid film and liquid slug is believed to be controlled by leakage flow and molecular diffusion (Sobieszuk et al., 2012; Yao et al., 2015b). As a result, the combination of enhanced transport phenomena (local mixing) and suppressed axial dispersion (backmixing) makes Taylor flow an ideal hydrodynamic regime for applications in gas-liquid two-phase systems.

In the development and design of microchannel devices for fast gas-liquid two-phase processes, it has been demonstrated that the mass transfer from gas bubbles to the surrounding liquid phase (bulk slugs and thin film) is an important limiting factor (Irandoust and Andersson, 1988; Kreutzer et al., 2001; van Baten and Krishna,

2004). Therefore, reliable determination of the liquid phase volumetric mass transfer coefficient (k_La), for gas-liquid mass transfer, becomes crucial to characterize this multiphase flow process.

Mass transfer in gas-liquid flow in microchannels has been intensively investigated with numerical and experimental methods, while a number of empirical or semi-theoretical correlations have also been proposed. Berčič and Pintar (1997) put forward an empirical correlation based on a unit cell model for predicting k_La in methane-water system. The unit cell was composed of a bubble and its adjacent slug, or a slug and its adjacent two half bubbles (Fig. 1). The offline experimental results, where the inlet and outlet effects were difficult to be eliminated, showed k_La to be mainly determined by two-phase superficial velocity and the length of unit cell:

$$k_L a = \frac{0.111(U_G + U_L)^{1.19}}{(1-\varepsilon_G)(L_G + L_S)^{0.57}} \tag{1}$$

Considering the contribution from two hemispherical caps and the thin liquid film surrounding the bubble, van Baten and Krishna (2004) adopted a more fundamental correlation based on the unit cell model and the unsteady-state diffusion model of Pigford:

$$k_L a = 2\frac{\sqrt{2}}{\pi}\sqrt{\frac{DU_B}{D_H}}\frac{4}{L_G + L_S} + \frac{2}{\sqrt{\pi}}\sqrt{\frac{DU_B}{\varepsilon_G(L_G + L_S)}}\frac{4\varepsilon_G}{D_H} \tag{2}$$

However, the correlation was based on a circular channel, thus not suitable for square channels because of the thicker liquid film (Han et al., 2011) and the intensive leakage flow in the corners (Yao et al., 2015b). On the basis of the experimental results, Yue et al. (2009) obtained an improved empirical correlation with reasonable

predicting accuracy in the square microchannel according to Eq. (2). Subsequently, a modified correlation was developed by Vandu et al. (2005) based on the correlation of van Baten and Krishna (2004) with the additional assumption that the main contribution to mass transfer was from the liquid film (Eq. (3)). This model was well supported by their experimental results for air-water system.

$$k_L a = \frac{4.5}{D_H}\sqrt{\frac{DU_G}{L_G + L_S}} \tag{3}$$

Although the above correlations based on the unit cell model were found to be in good agreement with their respective offline experimental results, they still face difficulties to fit to the processes of quick dissolution or high solubility of gases in liquids. The difficulties are mainly associated with the change in mass transfer due to gas solubility and the resulted evolution of the bubble volume along the microchannel. These changes can be pronounced in medium or high solubility system, such as CO_2-water, CO_2-amines (Abolhasani et al., 2012; Cubaud et al., 2012; Li et al., 2012).

In particular, CO_2-water system has been found suitable for studying gas-liquid mass transfer characteristics in microscale devices, even considered as a benchmark system (Yue et al., 2007; Sobieszuk et al., 2011; Yao et al., 2014a, 2014b). To enable the characterization of the system dynamics, much effort has been devoted to the development of online or *in situ* measurement methods employed (Abolhasani et al., 2012; Li et al., 2012; Tan et al., 2012; Cubaud et al., 2012; Yao et al., 2014a; Shim et al., 2014; Abolhasani et al., 2015). For example, Cubaud et al. (2012) experimentally examined the evolution of CO_2 bubbles dissolving in water using long serpentine microchannels, and individual bubbles along the flow direction were tracked to

establish the functional relationship between bubble size and velocity. For systematic and rapid investigation of CO_2 mass transfer and solubility in physical solvents, Abolhasani et al. (2012) proposed an automated microfluidic approach using high-speed photography method. The volumetric liquid phase mass transfer coefficients of CO_2-dimethyl carbonate system were estimated from the measured rate of bubble shrinkage with constant initial slug length. Subsequently, they took advantage of an image-based feedback strategy to automatically determine the length reduction of initially uniformly sized gas slugs at different positions along the microchannels and elucidate the gas concentration within adjacent liquid segments. Li et al. (2012) measured accurately the kinetics of fast gas-liquid reactions by online analysis of time-dependent changes in bubble size for CO_2-secondary amines system. Tan et al. (2012) obtained the overall mass transfer coefficient in the flowing stage by online measuring the change of gas slug volume versus flowing distance, and put forward semi-empirical equations based on the experimental results. Furthermore, a combined approach of the online high-speed photography and the unit cell model was adopted by Yao et al. (2014a), and the mass transfer was determined based on the absorption rate of CO_2 gas bubbles in water. However, there still remains a lack of understanding of the mechanism especially the dynamics details during the dissolution of gas bubbles and the evolution of k_La along microchannels (Abiev et al., 2017).

The aim of the present work was to quantitatively characterize the dynamic process of a gas-liquid system with medium gas solubility. Polymethyl methacrylate (PMMA)

microfluidic devices with long serpentine square microchannel were designed and fabricated having a range of channel geometries selected. An online measurement technique with a high-speed camera and a stereo microscope was employed to measure the evolution of the bubble size during CO_2 absorption process in water along the microchannel. A unit cell model was further combined with the online measurement to investigate the dynamics of gas-liquid two-phase mass transfer through the analysis of bubble and slug lengths. The influence of channel geometry was also studied on the volumetric mass transfer coefficient in a unit cell. Finally, the volumetric liquid phase mass transfer coefficients along the serpentine microchannel obtained experimentally in this work were compared with three correlations from the literature.

2. Experimental section

The schematic of the experimental setup is shown in Fig. 2(a). Two high pressure syringe pumps (LSP01-1BH, Longer) and two stainless steel syringes (full scale 50 mL, made in-house) were used to deliver gas and liquid, respectively. The liquid flow rate under each run was calibrated by weighing method, as well as the gas flow rate by automated electronic soap film flowmeter (GL-101B, 0.1~100 mL/min, accuracy of 1%, Beijing Beifen Sanpu, China). The gas and liquid flow rate were set in the range of 0.5~5.5 mL/min and 0.5~2.5 mL/min, respectively. Reynolds numbers were controlled in the range of 124~232. Pure CO_2 (99.999%) and deionized water were used as the working fluids. The operating temperature was set to 25 ^{o}C. The pressure drop for each run was measured by a pressure transducer (DMP305X, 0~50 kPa,

accuracy of 0.075%, LEEG, China). The dissolution of CO_2 bubbles was recorded by a high-speed video camera (Phantom R311, 2000 frames per second) mounted on a stereo microscope (Olympus SZX 16). The resolution and the shutter time were set as 1280×800 pixels and 490 μs, respectively. The imaging area covered all 12 serpentine microchannels and one typical captured image was shown in Fig. 2(b). One thousand sequence frames for each run were taken and the evolution of bubble lengths, velocities and their corresponding locations were analyzed by an image analysis program developed in Matlab®.

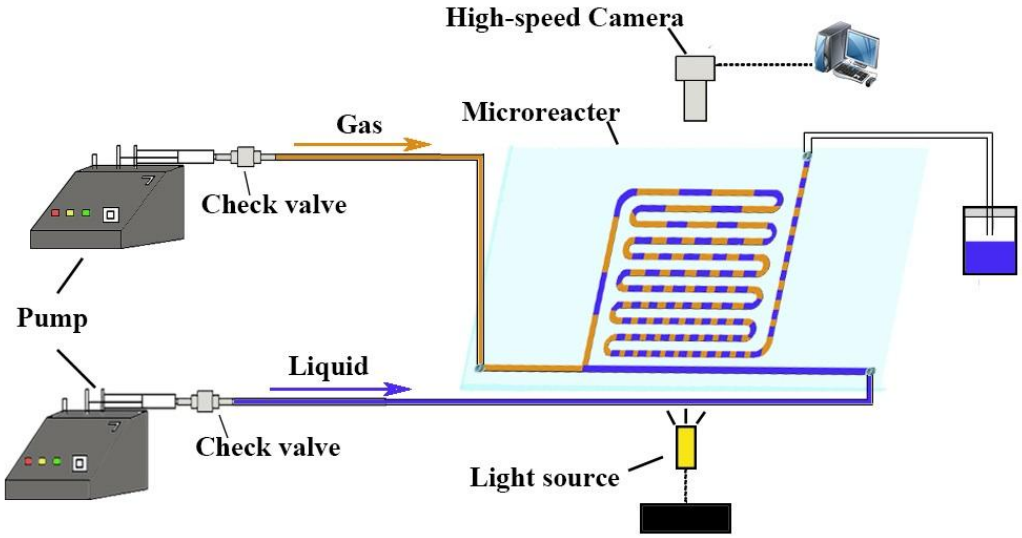

(a)

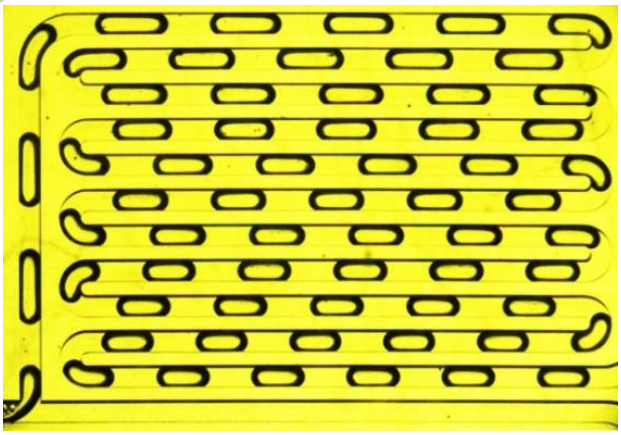

(b)

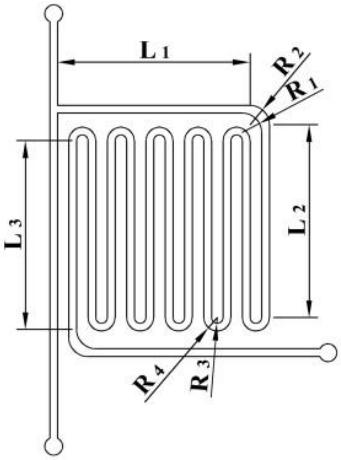

(c)

Fig. 2. Components of T-junction microchannel and gas-liquid mass transfer system (a) Schematic of the experimental setup; (b) Typical captured image; (c) T-junction microchannel

Fig. 2(c) shows a design of the T-junction microfluidic device with long serpentine microchannel used in this work, and the channel specifications are summarized in Table 1. These devices were fabricated on PMMA plates (A grade, 92% of light transmittance, ShenZhen HuiLi Acrylic Products Co., Ltd.) by precision milling technology and sealed by thermal sealing. To reduce the footprint of these devices, the long serpentine microchannels were made into multiple channels arranged in parallel and connected with circular bends.

Table 1

Channel geometric parameters

Width/w	L_1	L_2	L_3	R_1	R_2	R_3	R_4	Total length/L
				Mm				
0.4	9.98	14.38	13.96	1.0	1.5	0.3	0.7	181.63
0.6	9.43	14.28	13.96	1.0	1.5	0.2	0.8	181.13
0.8	16.1	14.08	13.26	1.0	1.5	0.4	1.2	189.88
1.0	16.6	13.98	13.26	1.0	1.5	0.3	1.3	190.28

3. Model for mass transfer coefficient

A unit cell model for Taylor flow was adopted in this work (van Baten and Krishna, 2004; Yao et al., 2014a), as shown in Fig. 1. The assumptions of the model are that: (i) gas and liquid phases are well-mixed in each unit cell; (ii) each unit cell is considered as a plug flow; (iii) mass transfer from gas to liquid phase only happens in a unit cell; (iv) the adjacent unit cells are mutually independent, where no mass transfer exists.

According to the above assumptions, the mass balance of CO_2 in the liquid phase

can be determined by:

$$\frac{dN_{CO_2}}{dt} = -k_L(C^{*L}_{CO_2} - C^{L}_{CO_2})A_S = -k_L a(C^{*L}_{CO_2} - C^{L}_{CO_2})(V_{CO_2} + V_L) \quad (4)$$

where $\frac{dN_{CO_2}}{dt}$ is mole variation rate of CO_2 in the gas phase, mol/s; k_L is the liquid phase mass transfer coefficient of the unit cell at a certain position along the serpentine microchannel, m/s; A_S is the effective mass transfer area in a unit cell, m^2; a is the specific surface area based on the liquid phase, m^2/m^3; V_{CO_2} is the gas phase volume in a unit cell, m^3; V_L is the liquid phase volume of the unit cell including liquid slug and film, m^3; $C^{*L}_{CO_2}$ is the equilibrium concentration of CO_2 in water with gas phase, mol/m^3; $C^{L}_{CO_2}$ is the CO_2 concentration in water along the serpentine microchannel, mol/m^3.

N_{CO_2} can be expressed by the ideal-gas equation:

$$N_{CO_2} = \frac{P_{CO_2} V_{CO_2}}{RT} \quad (5)$$

where P_{CO_2} is the gas phase pressure, Pa; R is the gas constant, 8.3145 J/(mol·K); T is the operating temperature, K.

Eq. (4) can be further rearranged to:

$$\frac{P_{CO_2}}{RT}\frac{dV_{CO_2}}{dt} = \frac{P_{CO_2}}{RT}\frac{dV_{CO_2}}{dX}U_B = -k_L a(C^{*,L}_{CO_2} - C^{L}_{CO_2})(V_{CO_2} + V_L) \quad (6)$$

where X denotes the distance from the T-junction, mm; U_B is the gas bubble velocity, m/s.

In the present work, the gas phase pressure is close to atmosphere pressure and $C^{*L}_{CO_2}$ can be determined by Henry's Law:

$$C_{CO_2}^{*\,L} = \frac{P_{CO_2}}{H_{CO_2}^{water}} \tag{7}$$

where $H_{CO_2}^{water}$ is Henry constant of CO_2 in water, $Pa \cdot m^3 \cdot mol^{-1}$, and can be determined by the following empirical correlation (Versteeg et al., 1988):

$$H_{CO_2}^{water} = 2.8249 \cdot 10^6 \exp(-\frac{2044}{T}) \tag{8}$$

The gas phase volume in a unit cell along a serpentine microchannel has been estimated by our previous research (Yao et al., 2015b):

$$V_{CO_2} = [(\pi - 4)I^2 + (D_H - 2\delta)^2](L_{CO_2} - D_H) + \frac{4}{3}\pi(0.5D_H - \delta)^3 \tag{9}$$

where I is the radius of the quadrant at the corner and can be obtained from the captured images, m; D_H is the hydraulic diameter, m; L_{CO_2} is the length of Taylor bubble from the captured images, m; δ denotes the liquid film thickness near the channel wall center and can be estimated by the correlation from Aussillous and Quéré (2000):

$$\delta = \frac{0.67Ca^{2/3}}{1 + 3.35Ca^{2/3}} D_H \tag{10}$$

where *Ca* is gas-liquid two-phase capillary number, defined as

$$Ca = \frac{\mu_L U_B}{\gamma_L} \tag{11}$$

where μ_L is the liquid phase viscosity, Pa·s; γ_L is the gas-liquid interfacial tension, N/m.

Theoretically, the radius of the quadrant should be changing along the microchannel. However, the variation of I values in the system examined was insignificant and undetectable with the imaging technique. Therefore, it is reasonably considered as a constant. The calculation of k_La was based on Eq. (6). Using 1,000

continuously captured images, V_{CO_2}, U_B and V_{CO_2}/dX can be calculated along the mirochannel. The CO_2 bubble volume (V_{CO_2}) in a unit cell along the serpentine microchannel was estimated from Eq. (9). The variation of CO_2 bubble volume was considered to be dissolved in the liquid phase. The liquid phase volume of the unit cell V_L was determined based on the frequencies of liquid slug formation. Thus, the concentration of CO_2 ($C^L_{CO_2}$) in the liquid phase was estimated because gas and liquid phases were well-mixed in each unit cell. The gas phase pressure P_{CO_2} was measured by a pressure transducer. The equilibrium concentration of CO_2 in water with gas phase $C^{*,L}_{CO_2}$ was calculated from Eq. (7). From Eqs. (6-11) and the captured images, the evolution of the volumetric liquid phase mass transfer coefficient k_La in a unit cell along the microchannel can be determined.

4. Results and Discussion

4.1. Gas bubble length and velocity

Fig. 3 shows the evolution of CO_2 Taylor bubble length along the serpentine microchannel at different gas flow rates for a given liquid flow rate, and at different liquid flow rate for a given gas flow rate. Both width and depth of the microchannel were 0.6 mm. The Taylor bubble length L_{CO_2} was measured between the tips of the two end-caps. The horizontal axis X indicates the axial distance from the T-junction along the serpentine microchannel.

The results (Fig. 3(a)) showed, at a given liquid flow rate of 2.0 mL/min, the Taylor bubble length L_{CO_2} decreased when flowing along the channel. That trend applied to all four selected gas flow rate levels, while increasing gas flow rate resulted in

increase in L_{CO_2} at both T-junction and along the microchannel. In contrast, at a given gas flow rate L_{CO_2} decreased with the increase of the liquid flow rate (Fig. 3(b)). In this section, the capillary numbers were low ($0.001<Ca<0.004$), so the formation of Taylor bubbles was believed to be controlled by the squeezing regime (Garstecki et al., 2006; Fu et al., 2015). However, as further increasing in capillary number to 0.707, the flow regime in the liquid slug changes from circulation flow to bypass flow (Abiev, 2009), which is beyond the scope of our work. In circulation flow regime, the Garstecki model or its modified model can be applied to predict the initial Taylor bubble size at the T-junction (Garstecki et al., 2006; Xu et al., 2008; Yao et al., 2015a).

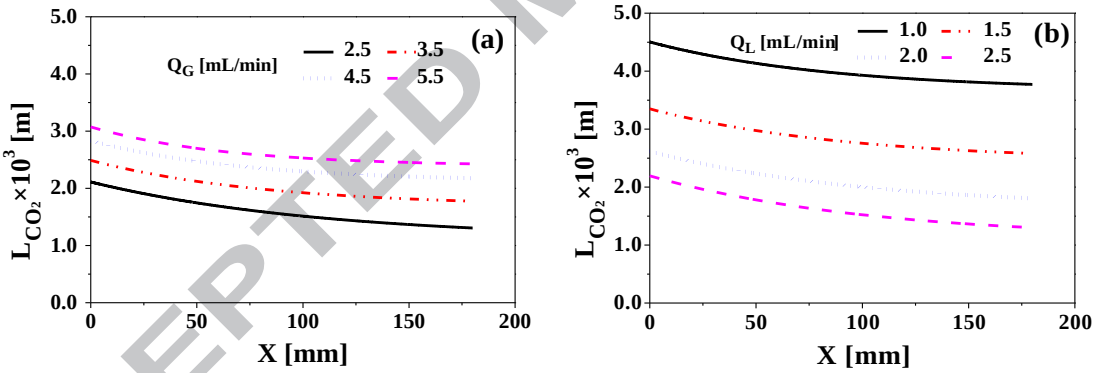

Fig. 3. The evolution of Taylor bubble length along the serpentine microchannel at 25 ^oC and 1.0 atm for Q_L= 2.0 mL/min (a) and Q_G= 3.5 mL/min (b)

It was also observed that the Taylor bubble shrunk through a two-stage process. At stage I, the volume of CO_2 bubbles has a rapid decrease within a short time following the bubble formation. At stage II, the shrinking rate gradually reduced and subsequently leveled off during flow along the microchannel. This was likely the results of the interplay of two competitive factors during the evolution of the bubbles along the microchannel, i.e., CO_2 dissolution and pressure drop. The CO_2 dissolution

into water can result in decrease in Taylor bubble length until the aqueous phase was saturated with CO_2. At the same time, the gas hold-up and pressure drop across this section changed accordingly. For example (at Q_G= 2.5 mL/min, Q_L=2.0 mL/min), the gas hold-up changed from 0.553 to 0.413, and the pressure drop varied from 2.0 kPa to 5.0 kPa, respectively. It is generally understood that the pressure drop is nonlinear with the length where both velocity and bubble length keep changing (Warnier et al., 2010). However, the pressure drop between inlet and outlet in our study was very low (the maximum pressure drop <6.6 kPa) and the microchannel length was relatively long (>250 mm). Therefore, the evolution of the local pressure along the microchannel was found to be insignificant. As a result, a linear correlation can be reasonably adopted in this work to represent the relationship between the pressure drop and the location along the flow direction. However, its effect on flow dynamics can be more complex than the CO_2 dissolution. On one hand, the reduction of the pressure drop along the flow direction induced expansion of the Taylor bubble. On the other hand, the increase of local pressure caused by the existence of pressure drop in the long microchannel was in favor of intensifying CO_2 dissolution processes. This suggested that the Taylor bubble length should firstly shrink and subsequently increase along the flow direction from the T-junction considering the pressure drop as only one factor.

Fig. 4 shows the effects of the gas (or liquid) flow rate on Taylor bubble velocity along the serpentine microchannel. The Taylor bubble velocity gradually decreased and subsequently reached a plateau along the channel. In this work, the solubility of

CO_2 in water was relatively low (~1.5 g/L) at 25 ^oC and 1 atm. Moreover, the density difference of the working fluids (CO_2 and water) was very large, while the liquid volume was to be appropriately constant over the course of CO_2 dissolution. Due to the decrease in Taylor bubble length during CO_2 absorption, the Taylor bubble velocity can inevitably be decelerated to compensate for the flux of CO_2 going into liquid phase, until the saturated solubility was reached (Abolhasani et al., 2012; Sun and Cubaud, 2011). The variation of the CO_2 concentration in liquid phase along the serpentine microchannel was shown in Fig.5. It could be seen that $C^{L}_{CO_2}$ was gradually close to the equilibrium concentration of CO_2 ($C^{*L}_{CO_2}$) in water with gas phase along the flow direction. In addition, accompanying with CO_2 dissolution in water along the flow direction, the CO_2 concentration in liquid phase was increased, which subsequently led to the decrease of the liquid phase absorption capacity and the interfacial concentration gradient. Thus, the slope of the evolution curve for the Taylor bubble velocity increases with the increase of the liquid flow rate, as shown in Fig. 4(b).

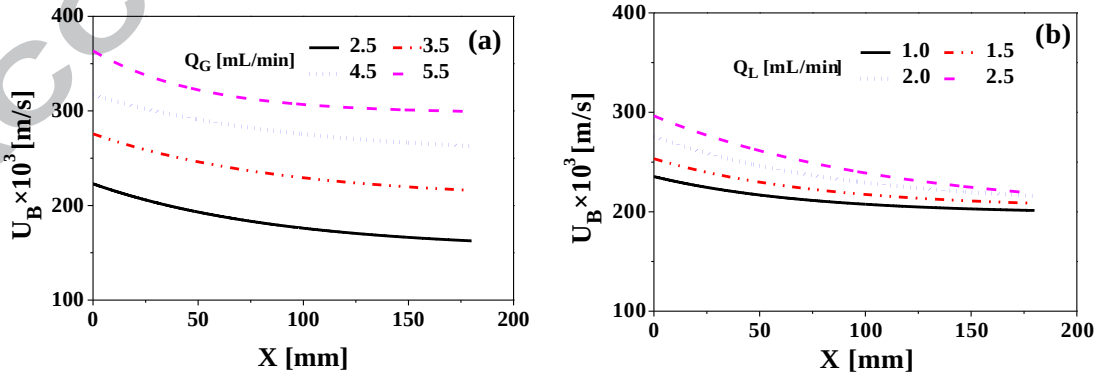

Fig. 4. The evolution of Taylor bubble velocity along the serpentine microchannel at 25 ^oC and 1.0 atm for Q_L= 2.0 mL/min (a) and Q_G= 3.5 mL/min (b)

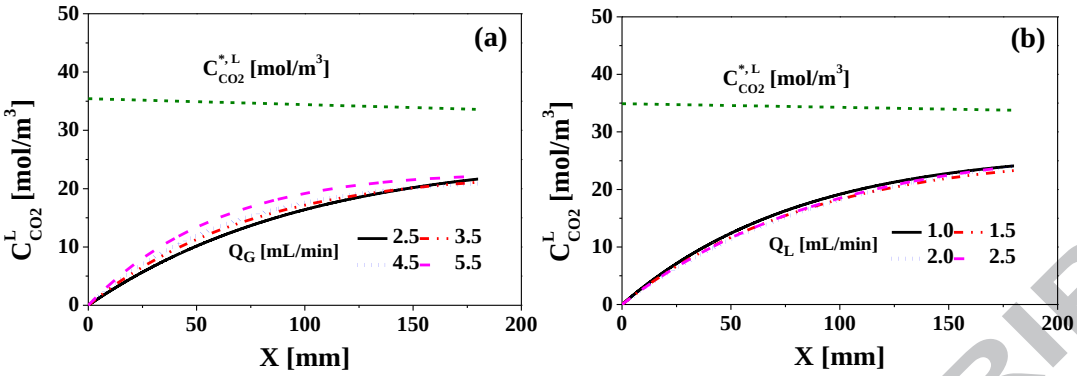

Fig. 5. The effects of the gas or liquid flow rate on the CO_2 concentration in water along the serpentine microchannel in a unit cell along the serpentine microchannel at 25 ^{o}C and 1.0 atm for Q_L= 2.0 mL/min (a) and Q_G= 3.5 mL/min (b)

4.2. Analysis of gas-liquid mass transfer process

The volumetric liquid phase mass transfer coefficients (k_La) were estimated according to Eq. (6). Accurate CO_2 bubble volume in a unit cell can be estimated even though the linear pressure distribution along the microchannel. The pressure at a certain position in the serpentine microchannel and the CO_2 saturation solubility were estimated with our experimental results. Reynolds numbers were in the range of 139~232. Fig. 6 shows the variation of k_La along the flow channel under a range of fluidic conditions.

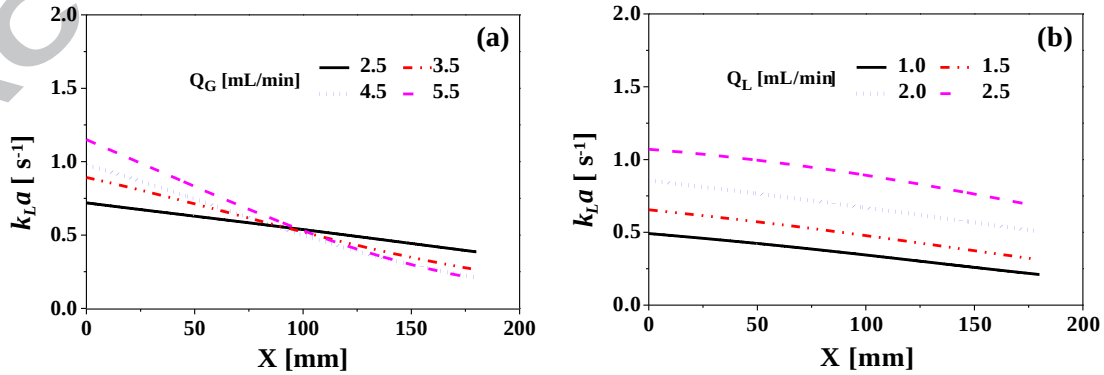

Fig. 6. The effects of the gas or liquid flow rate on the volumetric liquid phase mass transfer coefficient in a unit cell along the serpentine microchannel at 25 ^{o}C and 1.0 atm for Q_L= 2.0 mL/min (a) and Q_G= 3.5 mL/min (b)

Results showed the volumetric liquid phase mass transfer coefficient in a unit cell gradually decreased along the channel. As can be seen from Fig. 1, the mass transfer in a Taylor flow unit cell takes place (i) around the two hemispherical caps (end-caps) to the liquid slug, and (ii) across the sides of the Taylor bubble to the surrounding liquid film (Kreutzer, 2003; van Baten and Krishna, 2004). In a microchannel with square cross section, the liquid film can be further divided into two areas, at channel center and at four corners (Fig. 1(b)). As the film thickness (δ) at the center of the channel wall was much smaller than that at four corners (δ_{corner}), the liquid film at wall center can be saturated preferably compared to the liquid film at four corners and the liquid slug.

To what extent, whether the liquid film is saturated that can be determined from the *Fourier* number (Pohorecki, 2007), *Fo*, that is the ratio of the contact time of gas bubble with liquid film t_C to the time needed for liquid film saturation at wall center, t_S.

$$\mathrm{Fo} = \frac{\mathrm{t_C}}{\mathrm{t_S}} = \frac{\mathrm{L_{CO_2}} / \mathrm{U_B}}{\delta^2 / \mathrm{D}_{\mathrm{H_2O}}^{\mathrm{CO_2}}} \tag{12}$$

The resulting *Fo* numbers in our experiments are illustrated in Fig. 7 at varying flow rate levels. The low values of *Fo* number (< 0.75) indicated the liquid film at wall center to be less saturated.

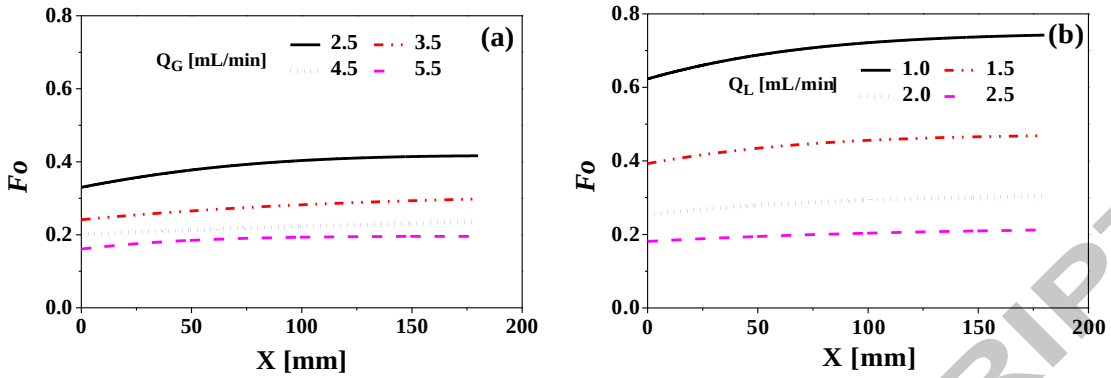

Fig. 7. The variation of *Fo* numbers along the serpentine microchannel at 25 ^{o}C and 1.0 atm for Q_L= 2.0 mL/min (a) and Q_G= 3.5 mL/min (b)

The contribution of the liquid film at wall center to the overall mass transfer in a unit cell is also important, where the contact area between the liquid film and the gas bubble in a unit cell is regarded as the effective mass transfer area. The overall effective mass transfer area can be determined according to the evolution of Taylor bubble using Eq. (12).

$$A_S = [2\pi I + 4(D_H - 2\delta - 2I)](L_{CO_2} - D_H) + 4\pi(0.5D_H - \delta)^2 \quad (12)$$

The effects of the gas flow rate on the specific interfacial area (a=A_S/(V_L+V_G) and the liquid phase mass transfer coefficient (k_L) in a unit cell along the serpentine microchannel were shown in Fig. 8(a) and Fig. 9(a), respectively. Also, the effects of the liquid flow rate at a given gas flow rate were shown in Fig. 8(b) and Fig. 9(b). The results showed that a and k_L gradually decreased along the serpentine microchannel. Due to the CO_2 absorption in water along the serpentine microchannel, the CO_2 bubble velocity decreased, and then the leakage flow in the liquid film and the circulation in the liquid slug became partly weakened (Yao et al., 2015b; Abolhasani et al., 2015), eventually, leading to the reduction in liquid phase mass transfer coefficient.

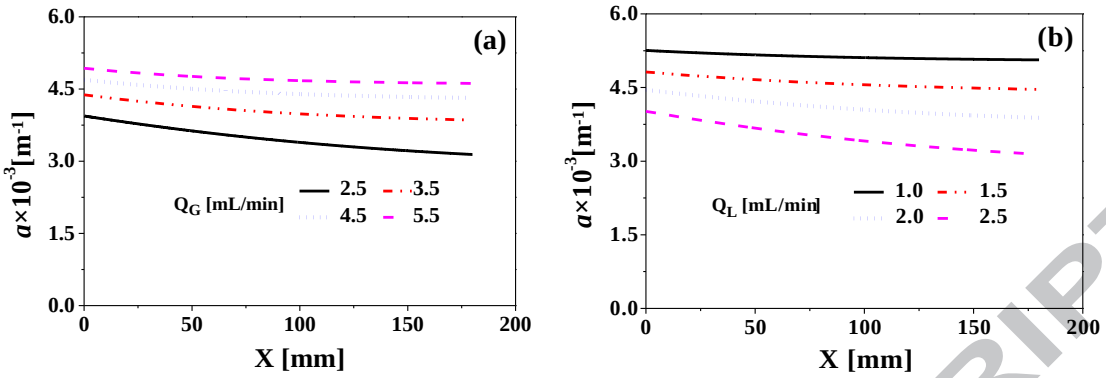

Fig. 8. The evolution of the specific interfacial area along the serpentine microchannel at 25 ^{o}C and 1.0 atm for Q_L= 2.0 mL/min (a) and Q_G= 3.5 mL/min (b)

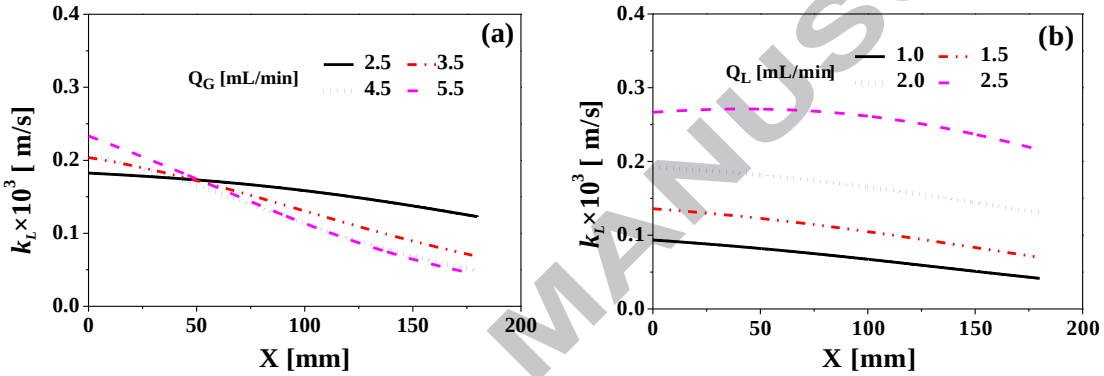

Fig. 9. The evolution of k_L along the serpentine microchannel at 25 ^{o}C and 1.0 atm for Q_L= 2.0 mL/min (a) and Q_G= 3.5 mL/min (b)

The decrease in the specific interfacial area was mainly induced by the reduction in CO_2 bubble length along the serpentine microchannel as a result of decrease in the liquid film length (Figs. 3 & 8). In addition, the slope of the specific interfacial area in Fig. 8(a) decreased gradually along the flow direction, indicating the shrinkage of the CO_2 bubble length being decelerated significantly by the CO_2 dissolution in water.

As seen in Fig. 9(a), there is a critical channel position (X = 40 mm) where the profile of liquid phase mass transfer coefficient k_L differs with varying gas flow rate at a given liquid flow rate. This is similar to the observation for k_La (Fig. 6(a)). In general, k_L in a unit cell is mainly determined by the surface renewal velocity of liquid phase, which is controlled by the circulation in the liquid slug and the leakage flow in

the liquid film. On one hand, the circulation in the liquid slug is intensified by reduction in liquid slug length due to the increase of the gas flow rate, which is in favor of the increase of k_L. On the other hand, the increase in Taylor bubble length can lead to the increase in liquid film length. This film length increase can further partly inhibit the liquid exchange between the liquid slug and the liquid film through the leakage flow in the film, especially in the four corners, resulting in k_L decrease. The experimental results (Fig. 9(a)) indicated that the contribution of the circulation in the liquid slug to k_L was dominant prior to the critical position compared to the leakage flow in the liquid film. On the contrary, with the accumulation of CO_2 concentration in the bulk slugs, the effects of the leakage flow in the liquid film on k_L were dominant after the critical point compared to the circulation in the liquid slug.

As shown in Fig. 3(a), for a unit cell at the same location along the flow direction, the length of the Taylor bubble increased with the increase of the gas flow rate, indicating an increase in the overall effective mass transfer area A_S. Moreover, the frequencies of liquid slug formation at the T-junction increased with increase in gas flow rate for a given liquid flow rate in our experiments, resulting in a decrease in liquid phase volume V_L. Thus, the specific interfacial area was enlarged intensively according to the evolution of A_S and V_L with the increase of the gas flow rate, as shown in Fig. 8(a). It was the results of the interplay of the above competitive factors that determined the overall volumetric mass transfer coefficient in a unit cell along the flow direction.

As discussed above, k_L was mainly controlled by the circulation in the liquid slug

and the leakage flow in the liquid film. The Taylor bubble length decreased with the increasing liquid flow rate, which led to the reduction in liquid film length. Thus, the liquid exchange between the liquid slug and the liquid film through the leakage flow in the film was enhanced, that further improved the liquid phase mass transfer coefficient. On the other hand, the liquid slug length also increased with increasing liquid flow rate at a given gas flow rate (Yao et al., 2013). That led to circulation weakened in the liquid slug. Our experimental results (Fig. 9(b)) suggested that the liquid phase mass transfer coefficient was largely controlled by the leakage flow in the liquid film under these operating conditions.

In addition, the increase in liquid flow rate caused the decrease in Taylor bubble length and, in turn, the overall effective mass transfer area for a given gas flow rate in a unit cell (Fig. 3(b) & Fig. 8(b)). Meanwhile, the volume of CO_2 bubble decreased in a unit cell. This can be attributed to the increasing liquid phase absorption capacity and the interfacial concentration gradient, which facilitated CO_2 absorption at the gas-liquid interface. So, the specific interfacial area decreased with increase in liquid flow rate (Fig. 8(b)). All the observation suggested that the contribution of the liquid phase mass transfer coefficient to the volumetric liquid phase mass transfer coefficient dominated over the specific interfacial area under the operating conditions investigated.

4.3. Effects of the channel geometry

The CO_2 absorption in water was carried out in square channels with different width (or depth), i.e. 0.4 mm, 0.6 mm, 0.8 mm and 1.0 mm. All these microchannels

had the same T-junction and channel length (Table 1). The ratio of the gas-liquid volumetric flow rate and Reynolds number (*Re*) at the entrance of the microchannels were kept constant. In general, the gas-liquid two-phase superficial velocity increased with the decrease in channel width under these operating conditions. This was also reflected by the evolution of the Taylor bubble velocity observed (Fig. 10(b)). The high liquid superficial velocity promoted the rupture of Taylor bubbles because of the rapid penetration of liquid phase into gas phase at the T-junction, where shorter CO_2 bubbles were created (Fig. 10(a)).

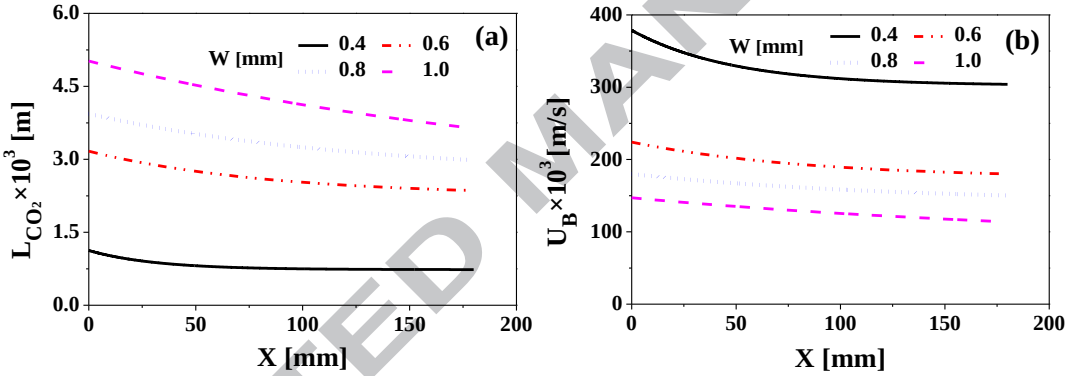

Fig. 10. The effects of channel geometry on the length (a) and the velocity (b) of Taylor bubble along the serpentine microchannel for Re=140 and Q_G/Q_L=0.5

The effects of microchannel geometry on mass transfer performance in these microchannels are presented in Fig. 11. The variations in k_La along flow direction in four channels showed a similar trend, i.e., k_La decreased when bubbles/slugs travelling down the channel. Moreover, k_La in a unit cell increased with decreasing channel hydraulic diameter. For the smallest channel the rate of decline in k_La was significantly greater than that of others before the critical point (X=120 mm). In this case, the fast CO_2 dissolution in water increased the CO_2 concentration in liquid phase at a higher rate towards the saturation of CO_2-water system in a shorter distance

(<120 mm).

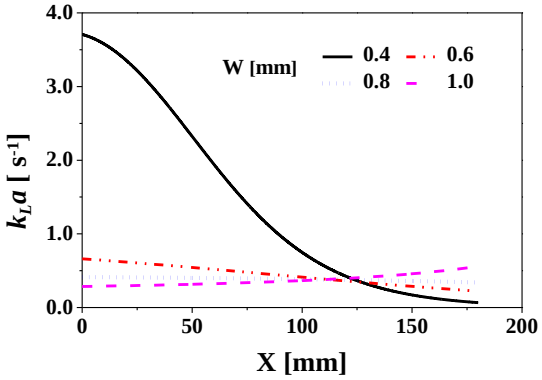

Fig. 11. The effects of channel geometry on k_La in a unit cell along the serpentine microchannel for Re=140 and Q_G/Q_L=1/2

k_La was affected by the variation of the length and velocity of Taylor bubble. A smaller size channel provided a short length but a higher velocity (Fig. 12), and subsequently, larger k_L and a. As a result, for a given Reynolds number, a larger number of Taylor bubbles were available in small microchannel compared to a large one for mass transfer. As discussed above, it can be deduced that the influence of the circulation in the liquid slug on k_L dominated over the leakage flow in the liquid film for 0.4 mm microchannel according to the results of Figs.10-12. The variation of Taylor bubble length and the effects of the leakage flow in the liquid film were mainly in the vicinity of the T-junction. Therefore, for k_L in this zone, its decrease caused by the decrease of the circulation in the liquid slug could be partly offset by the increasing of the leakage flow in the liquid film during absorption, and the variation of k_L appeared to be insignificant (Fig. 12). However, the slope of the evolution curve for k_La and k_L became larger when the Taylor bubble length was reduced to a certain extent, as shown in Figs.11 &12.

Furthermore, the interfacial area available for mass transfer increased. Moreover,

the internal circulation and the mixing in the liquid slugs were intensified due to the shorter liquid slugs (Su et al. 2012). Then, the surface renewal velocity of liquid phase was also enhanced which increased the concentration gradients at gas-liquid two-phase interface and further improved k_L. This indicated that k_L and a were all intensified by decreasing the channel size.

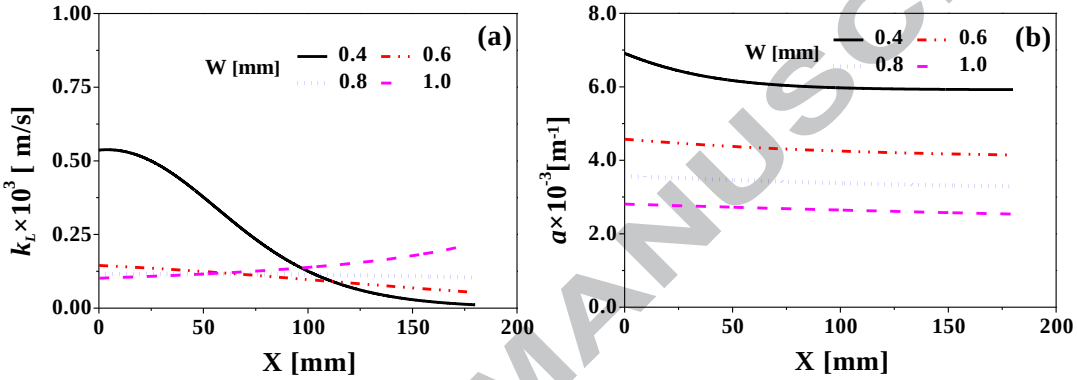

Fig. 12. The effects of channel geometry on k_L (a) and a (b) in a unit cell along the serpentine microchannel for Re=140 and Q_G/Q_L=0.5

4.4. Comparison of measured k_La with models from the literature

Fig. 13 compares the volumetric liquid phase mass transfer coefficients along the serpentine microchannel obtained experimentally in this work with that from three previously reported models. Two set of typical operational conditions were chosen for comparison. All previous models predicated approximate constant k_La along the serpentine microchannel. That was likely due to the key assumptions of these models with (i) constant Taylor bubble lengths, and (ii) constant k_La along their channels. However, the mass transfer is a dynamic process during gas-liquid Taylor flow where many parameters change such as bubble size, k_L and a along the microchannel. Thus, these models likely neglected the impact of such dynamic changes on two-phase mass transfer behavior. In addition, it is worthy of note that in our model the length of the

unit cell (L_G+L_S) was significantly lower (for at least one order of magnitude) than those used by the three previous models, that can improve the result accuracy.

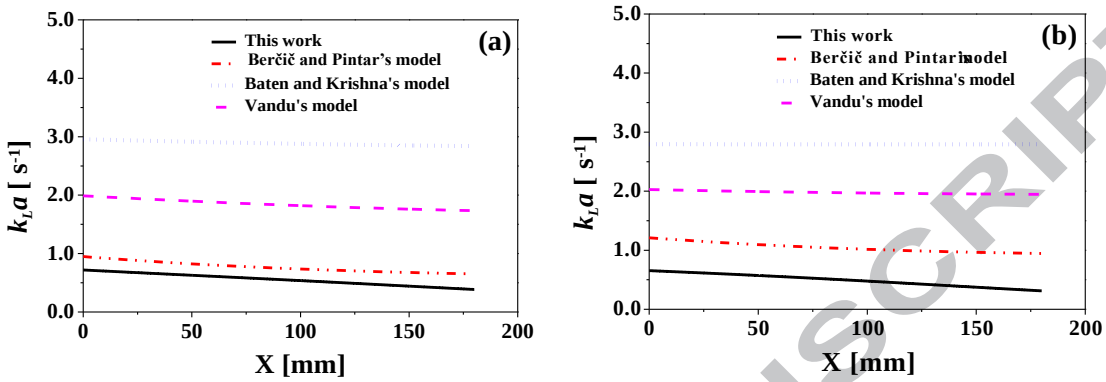

Fig. 13. Comparison of experimental k_La with those calculated by three correlations in the literature. (a) Q_L=2.0 mL/min, Q_G=2.5 mL/min, W=0.6 mm; (b) Q_L=1.5 mL/min, Q_G=3.5 mL/min, W=0.6 mm

5. Conclusions

An online high speed photography method and a unit cell model were introduced to investigate hydrodynamics variation and mass transfer characteristics of Taylor flow along long serpentine microchannel. It enabled quantitative characterization of the dynamic change of mass transfer along microchannel, by using volumetric mass transfer coefficients as transiently changing value for quantifying mass transfer process of CO_2 in water. Results showed that the Taylor bubble length shrunk and subsequently tended to plateau out along the flow direction from the T-junction, resulting in decrease in Taylor bubble velocity. The volumetric liquid phase mass transfer coefficient in a unit cell gradually decreased along the microchannel. As the gas flow rate increased under a given liquid flow rate, a critical point was found for the evolution of k_La and k_L. The results indicated that the contribution of the circulation in the liquid slug to k_L was dominant prior to the critical point compared to

the leakage flow in the liquid film. After the critical point, the leakage flow in the liquid film became the controlling factor. However, k_La and k_L increased with increasing liquid flow rate at a given gas flow rate. In principle, an expression or empirical correlation can act as a quantitative indicator for predicting the critical point. However, the existence of the critical point for k_L, which is mainly determined by the circulation in the liquid slug and the leakage flow in the liquid film, can be attributed to a number of factors, such as liquid viscosity, gas-liquid interfacial tension, liquid-solid surface tension, microchannel geometry, liquid velocity, and bubble velocity, etc. In order to elucidate the mechanism of such complex systems involving many influencing factors, further investigation is needed, which is ongoing in our laboratories. Regarding the effects of microchannel geometry, a small channel width was found in favor of intensifying gas-liquid two-phase mass transfer. Finally, the volumetric liquid phase mass transfer coefficients along the serpentine microchannel obtained experimentally in this work were compared with three previously reported models. It was found the previous models failed to predict the evolution, in particular, the variation of k_La along the serpentine microchannel. All these findings in this work provide important information to understand the dynamic change of gas-liquid Taylor flow mass transfer in microchannels. These can be potentially applied for designing and optimizing gas-liquid multiphase microreactors in the future.

Acknowledgments

We gratefully acknowledge the financial supports from National Natural Science Foundation of China (Nos. 21376234, 21676263, 21676230, U1662124) and State

Key Laboratory of Chemical Engineering (No. SKL-ChE-08A01).

Nomenclature

a	specific surface area, m^{-1}
A_S	effective mass transfer area in a unit cell, m^2
$C_{CO_2}^{L}$	CO_2 concentration in water along the serpentine microchannel, $mol \cdot m^{-3}$
$C_{CO_2}^{*\,L}$	equilibrium concentration of CO_2 in water with gas phase, $mol \cdot m^{-3}$
$D_{H_2O}^{CO_2}$	CO_2 diffusivity in water, $m^2 \cdot s^{-1}$
D_H	hydraulic diameter, m
$H_{CO_2}^{water}$	Henry constant of CO_2 in water, $Pa \cdot m^3 \cdot mol^{-1}$
I	radius of the quadrant at the corner, m
k_L	liquid phase mass transfer coefficient, $m \cdot s^{-1}$
L_{CO_2}	Taylor bubble length, m
L_G	bubble length in unit cell, m
L_S	liquid slug length in unit cell, m
N_{CO_2}	CO_2 in the gas phase, mol
P_{CO_2}	gas phase pressure, Pa
Q_G	gas flow rate, $m^3 \cdot s^{-1}$
Q_L	liquid flow rate, $m^3 \cdot s^{-1}$
R	gas constant, 8.3145 J/(mol·K)
T	operating temperature, K
U_G	superficial velocities of the gas phase, $m \cdot s^{-1}$
U_L	superficial velocities of the liquid phase, $m \cdot s^{-1}$
U_B	gas bubble velocity, $m \cdot s^{-1}$
V_{CO_2}	gas phase volume in a unit cell, m^3
V_L	liquid phase volume of a unit cell including liquid slug and film, m^3
t_C	contact time of Taylor bubble with the liquid film
t_S	liquid film saturation time at channel center
X	distance from the T-junction, mm
ε_G	gas hold-up
δ	liquid film thickness near the channel wall center, m
μ_L	liquid phase viscosity, Pa·s
γ_L	gas-liquid interfacial tension, $N \cdot m^{-1}$

Ca capillary number
Fo Fourier number
Re Reynolds number

References

Abiev, R.Sh., 2009. Circulation and bypass modes of the slug flow of a gas-liquid mixture in capillaries. Theor. Found. Chem. Eng. 43(3), 298-306.

Abiev, R.Sh., Svetlov, S., Hasse, S., 2017. Hydrodynamics and mass transfer of gas-liquid and liquid-liquid Taylor flow in microchannels. Chem. Eng. Technol. 40(11), 1985-1998.

Abolhasani, M., Singh, M., Kumacheva, E., Günther, A., 2012. Automated microfluidic platform for studies of carbon dioxide dissolution and solubility in physical solvents. Lab Chip 12(9), 1611-1618.

Abolhasani, M., Kumacheva, E., Günther, A., 2015. Peclet number dependence of mass transfer in microscale segmented gas-liquid flow. Ind. Eng. Chem. Res. 54(36), 9046-9051.

Aussillous, P., Quéré, D., 2000. Quick deposition of a fluid on the wall of a tube. Phys. Fluids 12(10), 2367-2371.

van Baten, J.M., Krishna, R., 2004. CFD simulations of mass transfer from Taylor bubbles rising in circular capillaries. Chem. Eng. Sci. 59(12), 2535-2545.

Berčič, G., Pintar, A., 1997. The role of gas bubbles and liquid slug lengths on mass transport in the Taylor flow through capillaries, Chem. Eng. Sci. 52(21-22), 3709-3719.

Cubaud, T., Sauzade, M., Sun, R.P., 2012. CO_2 dissolution in water using long serpentine microchannels. Biomicrofluidics 6(2), 022002.

Fu, T.T., Ma, Y.G., 2015. Bubble formation and breakup dynamics in microfluidic devices: A review. Chem. Eng. Sci. 135, 343-372.

Garstecki, P., Fuerstman, M.J., Stone, H.A., Whitesides, G.M., 2006. Formation of droplets and bubbles in a microfluidic T-junction-scaling and mechanism of break-up. Lab Chip 6(3), 437-446.

Gemoets, H.P.L., Su, Y.H., Shang, M.J., Hessel, V., Luque, R., Noël, T, 2016. Liquid phase oxidation chemistry in continuous flow microreactors. Chem. Soc. Rev. 45(1), 83-117.

Günther, A., Jensen, K.F., 2006. Multiphase microfluidics: from flow characteristics to chemical and materials synthesis. Lab Chip 6(12), 1487-1503.

Han, Y., Shikazono, N., Kasagi, N., 2011. Measurement of liquid film thickness in a micro parallel channel with interferometer and laser focus displacement meter. Int. J. Multiphase Flow 37(1), 36-45.

Hessel, V., Angeli, P., Gavriilidis, A., Löwe, H., 2005. Gas-liquid and gas-liquid-solid microstructured reactors: contacting principles and applications. Ind. Eng. Chem. Res. 44(25), 9750-9769.

Irandoust, S., Andersson, B., 1988. Mass-transfer and liquid-phase reactions in a segmented two-phase flow monolithic catalyst reactor. Chem. Eng. Sci. 43(8), 1983-1988.

Jia, H.W., Zhang, P., 2016. Investigation of the Taylor bubble under the effect of dissolution in microchannel. Chem. Eng. J. 285, 252-263.

Kashid, M.N., Renken, A., Kiwi-Minsker, L., 2011. Gas-liquid and liquid-liquid mass transfer in microstructured reactors. Chem. Eng. Sci. 66(17), 3876-3897.

Kececi, S., Wörner, M., Onea, A., Soyhan H.S., 2009. Recirculation time and liquid slug mass transfer in co-current upward and downward Taylor flow. Catal. Today 147, S125-S131.

Kreutzer, M.T., Du, P., Heiszwolf, J.J., Kapteijn, F., Moulijn, J.A., 2001. Mass transfer characteristics of three-phase monolith reactors. Chem. Eng. Sci. 56(21-22), 6015-6023.

Kreutzer, M.T., 2003. Hydrodynamics of Taylor flow in capillaries and monolith reactors. Ph.D. Thesis, Delft University of Technology, Delft, The Netherlands.

Li, L., Yao, C.Q., Jiao, F.J., Han, M., Chen, G.W., 2017. Experimental and kinetic study of the nitration of 2-ethylhexanol in capillary microreactors. Chem. Eng. Process.: Process Intensification 117, 179-185.

Li, W., Liu, K., Simms, R.W., Greener, J., Jagadeesan, D., Pinto, S., Günther, A., Kumacheva, E. A., 2012. Microfluidic study of fast gas-liquid reactions. J. Am. Chem. Soc. 134(6), 3127-3132.

Pedersen, H., Horváth, C., 1981. Axial dispersion in a segmented gas-liquid flow. Ind. Eng. Chem.

Fundam. 20(3), 181-186.
Pohorecki, R., 2007. Effectiveness of interfacial area for mass transfer in two-phase flow in Microreactors. Chem. Eng. Sci. 62, 6495-6498.
Salman, W., Gavriilidis, A., Angeli, P., 2007. Axial mass transfer in Taylor flow through circular microchannels. AIChE J. 53(6), 1413-1428.
Shao, N., Gavriilidis, A., Angeli, P., 2009. Flow regimes for adiabatic gas-liquid flow in microchannels. Chem. Eng. Sci. 64(11), 2749-2761.
Shim, S., Wan, J.D., Hilgenfeldt, S., Panchal, P.D., Stone, H.A., 2014. Dissolution without disappearing: multicomponent gas exchange for CO_2 bubbles in a microfluidic channel. Lab Chip 14(14), 2428-2436.
Sobieszuk, P., Pohorecki, R., Cyganski, P., Grzelka, J., 2011. Determination of the interfacial area and mass transfer coefficients in the Taylor gas–liquid flow in a microchannel. Chem. Eng. Sci. 66(23), 6048-6056.
Sobieszuk, P., Aubin, J., Pohorecki, R., 2012. Hydrodynamics and mass transfer in gas-liquid flows in microreactors. Chem. Eng. Technol. 35(8), 1346-1358.
Sobieszuk, P., Napieralska, K., 2016. Investigations of mass transfer in annular gas-liquid flow in a microreactor. Chem. Eng. Process. 37(1), 55-64.
van Steijn, V., Kreutzer, M.T., Kleijn, C.R., 2007. μ-PIV study of the formation of segmented flow in microfluidic T-junctions. Chem. Eng. Sci. 62(24), 7505-7514.
Su, Y.H., Chen, G.W., Yuan, Q., 2012. Influence of hydrodynamics on liquid mixing during Taylor flow in a microchannel. AIChE J. 58(6), 1660-1670.
Sun, R., Cubaud, T., 2011. Dissolution of carbon dioxide bubbles and microfluidic multiphase flows. Lab Chip 11(17), 2924-2928.
Tan, J., Lu, Y.C., Xu, J.H., Luo, G.S., 2012. Mass transfer performance of gas-liquid segmented flow in microchannels. Chem. Eng. J. 181, 229-235.
Vandu, C.O., Liu, H., Krishna, R., 2005. Mass transfer from Taylor bubbles rising in single capillaries, Chem. Eng. Sci. 60(22), 6430-6437.
Versteeg, G. F., van Swaaij, W.P.M., 1988. Solubility and diffusivity of acid gases (CO_2, N_2O) in aqueous alkanolamine solutions. Chem. Eng. J. 33(1), 29-34.
Warnier, M.J.F., de Croon, M.H.J.M., Rebrov, E.V., Schouten, J.C., 2010. Pressure drop of gas-liquid Taylor flow in round micro-capillaries for low to intermediate Reynolds numbers. Microfluid Nanofluid, 8, 33-45.
Xu, J.H., Li, S.W., Tan, J., Luo, G.S., 2008. Correlation of droplet formation in T-junction microfluidic devices: from squeezing to dripping. Microfluid. Nanofluid. 5(6),711-717.
Yang, L., Tan, J., Wang, K., Luo, G.S., 2014. Mass transfer characteristics of bubbly flow in microchannels. Chem. Eng. Sci. 109, 306-314.
Yao, C.Q., Zhao, Y.C, Ye, C.B., Dang, M.H., Dong, Z.Y., Chen, G.W., 2013. Characteristics of slug flow with inertial effects in a rectangular microchannel. Chem. Eng. Sci. 95, 246-256.
Yao, C.Q., Dong, Z.Y., Zhao, Y.C., Chen, G.W., 2014a. An online method to measure mass transfer of slug flow in a microchannel. Chem. Eng. Sci. 112, 15-24.
Yao, C.Q., Dong, Z.Y., Zhao, Y.C., Chen, G.W., 2014b. The effect of system pressure on gas-liquid slug flow in a microchannel. AIChE J. 60(3), 1132-1142.
Yao, C.Q., Dong, Z.Y., Zhao, Y.C., Chen, G.W., 2015a. Gas-liquid flow and mass transfer in a microchannel under elevated pressures. Chem. Eng. Sci. 123, 137-145.
Yao, C.Q., Dong, Z.Y., Zhang, Y.C., Mi, Y., Zhao, Y.C., Chen, G.W., 2015b. On the leakage flow around gas bubbles in slug flow in a microchannel. AIChE J. 61(11), 3964-3972.
Yue, J., Chen, G.W., Yuan, Q., Luo, L.A., Gonthier, Y., 2007. Hydrodynamics and mass transfer characteristics in gas-liquid flow through a rectangular microchannel. Chem. Eng. Sci. 62(7), 2096-2108.
Yue, J., Luo, L.A., Gonthier, Y., Chen, G.W., Yuan, Q., 2008. An experimental investigation of gas–liquid two-phase flow in single microchannel contactors. Chem. Eng. Sci. 63(16), 4189-4202.
Yue, J., Luo, L.A., Gonthier, Y., Chen, G.W., Yuan, Q., 2009. An experimental study of air-water Taylor flow and mass transfer inside square microchannels. Chem. Eng. Sci. 64(16), 3697-3708.
Zhao, Y.C., Chen, G.W., Ye, C.B., Yuan, Q., 2013. Gas-liquid two-phase flow in microchannel at elevated pressure. Chem. Eng. Sci. 87, 122-132.

Highlights

- Hydrodynamics variation and mass transfer characteristics of Taylor flow in a square cross-sectional microchannel are investigated
- An online high-speed imaging method and the unit cell model are adopted
- $k_L a$ decreases along the serpentine microchannel
- As the gas flow rate increases under a given liquid flow rate, a critical point is found for the evolution of $k_L a$ and k_L.